Some effects of flow expansion on the aerodynamics of horizontal-axis wind turbines

David H. Wood[1] and Eric J. Limacher[2]

[1]Department of Mechanical and Manufacturing Engineering, University of Calgary, Calgary T2N 1N4, AB, Canada.
[2]Department of Mechanical Engineering, Federal University of Pará, Belém, Brazil

Correspondence: David H. Wood (dhwood@ucalgary.ca)

Abstract. The flow upwind of an energy-extracting horizontal-axis wind turbine expands as it approaches the rotor, and the expansion continues in the vorticity-bearing wake behind the rotor. The upwind expansion has long been known to influence the axial momentum equation through the axial component of the pressure, although the extent of the influence has not been quantified. Starting with the impulse analysis of Limacher & Wood (2020), but making no further use of impulse techniques, we derive its exact expression when the rotor is a circumferentially uniform disc. This expression, which depends on the radial velocity and the axial induction factor, is added to the thrust equation containing the pressure on the back of the disk. Removing the pressure to obtain a practically useful equation shows the axial induction in the far-wake is twice the value at the rotor only at high tip speed ratio and only if the relationship between vortex pitch and axial induction in non-expanding flow carries over to the expanding case. At high tip speed ratio, we assume that the expanding wake approaches the "Joukowsky" model of a hub vortex on the axis of rotation and tip vortices originating from each blade. The additional assumption that the helical tip vortices have constant pitch, allows a semi-analytic treatment of their effect on the rotor flow. Expansion modifies the relation between the pitch and induced axial velocity so that the far-wake area and induction are significantly less than twice the values at the rotor. There is a moderate decrease – about 6% – in the power production and a similar size error occurs in the familiar axial momentum equation involving the axial velocity.

1 Introduction

Conservation of axial and angular momentum are fundamental principles for wind turbine analysis. They are applied using control volumes (CVs) such as those in figure 1, or more commonly, to a CV coinciding with a mean streamtube and extending into the far-wake, the hypothetical region of no further wake development. For blade-element momentum theory, the CVs become expanding annular streamtubes intersecting the elements. The change in axial or angular momentum of the flow determines the net thrust or torque, respectively, acting on the rotor or blade elements, e.g. Burton et al. (2011), Hansen (2015), and Sørensen (2016). Angular momentum is easier to analyze because in most cases it is generated only at the blades.

When a turbine extracts kinetic energy from the wind, the flow must expand both upwind and downwind of the rotor. As noted on p. 185 of Glauert (1935), and by Goorjian (1972), the axial momentum equation may receive contributions from the pressure in the expanding flow upwind of the rotor. The expansion causes the pressure force to have an axial component
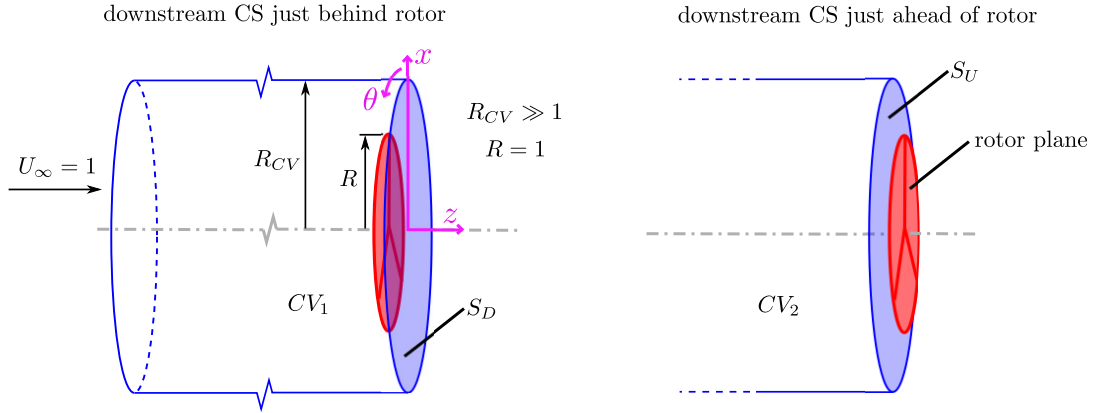
Figure 1. Control volumes (CVs) to be used in the present analysis. In both variants, the upstream face extends in z to $-\infty$, where the velocity is the wind speed, and $R_{CV} \gg R$. The downstream control surface is just downstream and just upstream of the rotor plane in CV_1 and CV_2, respectively, and the corresponding donwstream control surfaces (CS) are labelled S_D and S_U. Taken from LW.

25   which alters the rotor thrust by an amount equal to the momentum flux external to the rotor. This is because the pressure forces acting on the cylindrical control surfaces at radius R_{CV} in figure 1 are entirely radial. Although the role of pressure has been recognized for a long time, and is discussed by Sørensen (2016) and van Kuik (2018) among others, a satisfactory analysis of it is lacking. The first main result of the present analysis a closed-form expression for the pressure force for a circumferentially uniform rotor.

30   Limacher & Wood (2020) (hereinafter "LW") investigated steady wind turbine thrust, T, using an impulse analysis, whereby the pressure in the axial momentum equation for any CV is replaced by terms that include vorticity fluxes across the CV boundaries. This removal of pressure is achieved by the substitution of various integral identities into a standard momentum-based control volume analysis, as demonstrated by Noca (1997). We will use what we call the "impulse perspective" as explained below, but not impulse techniques in this paper; the interested reader is referred to LW for a short history and more

35   details. LW showed that by approximating a rotor as an actuator disc, T is given exactly by integration over the face S_D of CV_1, situated just downwind of the rotor on the left of figure 1:

$$\frac{T}{\rho} = \int_{S_D} \left(\frac{1}{2} w^2 + \lambda w x \right) dS. \tag{1}$$

where ρ is the air density, and w is the circumferential velocity (in the direction of θ in Figure 1) on S_D; in LW, w denoted the circumferential velocity at the rotor plane, which was assumed to be one half that on S_D. This assumption is also used in

40   the present analysis. λ is the tip speed ratio ($\lambda > 0$ for clockwise rotation, as viewed from positive z-axis), and x is the radius normalized by the tip radius so that $x \leq 1$ for the rotor. The downwind face of the second CV in the figure, S_U, is just upwind of the rotor. The term "exact" will be used throughout this paper to indicate that no assumptions beyond those listed below have been invoked. Taking the "wake" to be the flow that has passed through the rotor, which rotates with a constant angular velocity, these assumptions are:

45   1. the flow upwind of the rotor and outside the wake, is inviscid, steady, and spatially uniform,

2. the total energy of the wake is reduced instantaneously at the rotor, after which it is conserved,

3. viscous and/or Reynolds stresses can be neglected on the CV surfaces,

4. the axial, u, and radial velocity, v, are continuous through the rotor disk,

5. viscous drag is negligible,

50   6. w is zero in the upwind flow and outside the wake,

7. the vorticity in the wake is concentrated in line vortices or vortex sheets aligned with the local streamlines in the rotating frame of reference. In other words, the wake vortices rotate rigidly with the blades and vortex lines and streamlines coincide, and

8. to derive the local or differential form of Equation (1), the vorticity piercing the lateral boundaries of the annular CVs
55   intersecting the blade elements must have no effect on the element's thrust.

Assumption #7 simplifies the terms involving the trailing vorticity crossing S_D in the impulse derivation. Assumptions #3, #5, and #8 are likewise embedded in the equations derived by LW, and are not explicitly required in the analysis to follow. As LW note, a thorough investigation of assumption #8 remains an important area of future research, but as yet the assumption remains necessary to recover the Kutta-Joukousky expression for local thrust that is conventionally employed in blade-element
60   momentum (BEM) analyses. As such, we perpetuate the use of assumption #8 for the time being. We also note, emphatically, that none of the eight assumptions places any restrictions on flow expansion. Since the impulse derivation of (1) is likewise unrestricted, the equation is exact in the presence of flow expansion and for any distribution of $w(x)$.

Although Equation (1) has been known since Glauert (1935), and appears in modern texts, such as Equation (4.6) in van Kuik (2018), LW's analysis provides the first proof of its exactness when the trailing vortex sheets have finite thickness. LW's
65   second main finding for circumferentially-uniform, expanding flow, is

$$0 = \int_{S_U} \left(v^2 - a^2 \right) dS = \int_{S_D} \left(v^2 - a^2 \right) dS \tag{2}$$

where $a = 1 - u$ (when u is normalized by the wind speed, U_0) is the usual axial induction factor. To maintain consistency we use only normalized velocities from here on. The easiest was to do this is to mentally replace the density ρ by ρU_0^2.

van Kuik (2020) found Equation (2) was satisfied by his model of the expanding flow through a wind turbine rotor. When
70   a and v are further assumed to be C_0-continuous on S_U and S_D, Equation (2) tells us that $|a| = |v|$ at some radial location, and LW cite three simulations that show $|a| \approx |v|$ near the rotor tip. The vanishing of the first integral on S_U in (2) is the more general result; the vanishing of the second integral on S_D follows from assumption #4 above. Until the end of Section 3, we treat the rotor as circumferentially uniform. Since Equation (1) contains no terms representing pressure redistribution, LW

assert that its local version giving the contribution to the thrust at radius x, is also exact:

$$75 \quad \frac{1}{\rho}\frac{dT}{dx} = \int\limits_{0}^{2\pi} \left(\frac{1}{2}w^2 + \lambda w x\right) x\,d\theta = 2\pi w x \left(\frac{w}{2} + \lambda x\right), \tag{3}$$

where θ is the circumferential co-ordinate, defined in Figure 1. This result is also not new: it is, for example, Equation (4.24) of van Kuik (2018). It is often referred to as the "Kutta-Joukowsky" theorem for blade element thrust because it gives the axial force, dT/dx, as the product of the circumferential velocity *at the rotor*, $w/2 + \lambda x$, and the sum of the circulation on all blades, $2\pi w x$. Impulse analysis, however, can also be applied if the CV outlet is moved to the far-wake to give dT/dx in terms of the w in the far-wake. Glauert's (1935) original derivation of Equation (1) – based on the Bernoulli equation – also suggests the exactness of (3).

Equation (2) can be derived using standard CV momentum analysis, but the authors are unaware of it appearing in the literature prior to LW. It is a natural outcome of the impulse perspective which we use to investigate the effects of flow expansion on the conventional axial momentum equation. It will be shown that (2) is closely related to the effects of pressure in the upwind flow on the conventional axial momentum equation, and the general relationship between a and the far-wake induction, a_∞. T is derived in Chapter 4 of Sørensen (2016) and Section 5.2.4 of van Kuik (2018) using a CV ending in the far-wake. We take the different approach of using the CVs shown in Figure 1 because that choice clarifies the effects of expansion. We also make further use of the impulse form of the T equation. The derivations of the remaining equations in this paper are straightforward, and could have been easily done in the past if the impulse perspective had been available.

For context, we now examine the connection between the impulse- and momentum-based approaches to turbine thrust which requires a relationship between a and w. As explained by, for example, Wood et al. (2021), the Kawada-Hardin (KH) equations for the velocity field of a constant pitch, p, constant radius helical vortex, Kawada (1936), Hardin (1982), yield

$$\frac{p}{x} = \frac{w/2}{a}, \tag{4}$$

as only half of the near-wake azimuthal velocity is induced by the wake (the other half is due to the blades). Pitch can also be related geometrically to a and λ by treating the wake as a non-expanding rigid helicoidal surface, as done by Okulov and Sørensen (2008). In the limit where $\lambda x \gg w$, we have

$$\frac{p}{x} \approx \frac{1-a}{\lambda x}, \tag{5}$$

and the preceding two equations can be combined to give $\lambda w x \approx 2a(1-a)$. The high-$\lambda$ limit of equation (3) thus becomes

$$\left.\frac{1}{\rho}\frac{dT}{dx}\right|_{\lambda\to\infty} \approx 2\pi\lambda w x^2 \approx 4a(1-a)\pi x, \tag{6}$$

recovering the familiar $4a(1-a)$ integrand from classical momentum theory. At smaller λ, the relationship between the momentum- and impulse-based thrust expressions has not been fully investigated.

In the next section, we express the contribution of pressure on the expanding upstream streamtube to actuator disk thrust. The section thereafter analyzes the local form of the thrust equation. It contains our second main result about the behaviour

of a, that it is negligible at $\lambda = 0$ and $a_\infty \approx 2a$ is possible at high λ *only if* Equation (4) remains valid for expanding flow. In Section 4, we apply the Biot-Savart law to an expanding Joukowsky wake which contains only hub and tip vortices. On the further assumption of constant p, we show, again for the first time, that $a \leq a_\infty \leq 2a$ depending on the extent of the vortex expansion; the larger the expansion, the closer a approaches a_∞. Not surprisingly, the far-wake radius is reduced as is the power extracted by the turbine. The final two sections contain the general discussion and conclusions, respectively.

2 Actuator disk thrust for expanding flow

Some results of the impulse analysis can be converted easily to conventional equations containing the axial velocity and the pressure on the CV surface even when the flow expands through the rotor. For example, Bernoulli's equation for P_U, the pressure on S_U, is

$$\frac{2P_U}{\rho} = 1 - v^2 - u^2 \tag{7}$$

P_U and all pressures considered herein are gauge pressures relative to the free-stream pressure in the wind. Equation (7) allows the removal of v^2 from (2) to give

$$\int\limits_0^\infty \frac{P_U}{\rho} x dx = \int\limits_0^\infty u\left(1 - u\right) x dx \tag{8}$$

which is also the outcome of a conventional momentum balance on CV_2. The momentum balance on CV_1 yields

$$\frac{T}{2\pi\rho} = \int\limits_0^\infty u\left(1 - u\right) x dx - \int\limits_0^\infty \frac{P_D}{\rho} x dx. \tag{9}$$

where P_D is the pressure on S_D. It is important to note that the effective upper limit on the integrals in (9) is outside the rotor. Nevertheless,

$$\frac{T}{2\pi\rho} = \int\limits_0^1 \frac{P_U - P_D}{\rho} x dx = \int\limits_0^1 \frac{\Delta P}{\rho} x dx \tag{10}$$

since $P_D = P_U$ for $x > 1$. In other words, there is no pressure jump at $z = 0$ outside the rotor. The thrust equation with integration only over the rotor, can be found by rewriting (9) as

$$\frac{T}{2\pi\rho} = \int\limits_0^1 a\left(1 - a\right) x dx - \int\limits_0^1 \frac{P_D}{\rho} x dx + \int\limits_1^\infty a\left(1 - a\right) x dx - \int\limits_1^\infty \frac{P_D}{\rho} x dx. \tag{11}$$

To remove the last two integrals for $x \geq 1$, we use Equation (7) for $P_D = P_U$ and then (2), to arrive at

$$\frac{T}{\pi\rho} = 2\int\limits_0^1 a\left(1 - a\right) x dx - 2\int\limits_0^1 \frac{P_D}{\rho} x dx + \int\limits_0^1 \left(a^2 - v^2\right) x dx. \tag{12}$$

5

The first integral in (12) contributes half the conventional thrust. It and the second integral are components of conventional CV analysis, whereas the third integral is new. It makes (12) exact for an actuator disk when the flow expands and will be shown below to be generally positive. We now change the CV from that shown in figure 1 to the more commonly-used one formed by the bounding streamsurface (BS) dividing the flow passing through the rotor from the external flow. BS begins at $z = -\infty$ where z is the axial co-ordinate with origin at the rotor, figure 1. The vertical faces of the new CV are, therefore, subsets of those shown in figure 1. A straightforward momentum balance gives

$$\frac{T}{\pi\rho} = 2\int_0^1 a\left(1-a\right)x dx - 2\int_0^1 \frac{P_D}{\rho} x dx + 2\int_{-\infty}^0 \left(P\frac{dx}{dz}\right)_{BS} x dz \tag{13}$$

where the last integrand is evaluated on BS. dx/dz gives the local slope of BS, so Pdx/dz gives the axial component of the pressure acting on BS. It follows immediately from (12) and (13) that

$$\int_{-\infty}^0 \left(P\frac{dx}{dz}\right)_{BS} x dz = \frac{1}{2}\int_0^1 \left(a^2 - v^2\right) x dx \tag{14}$$

which gives the first quantification known to the authors of the axial force due to the expanding flow through a wind turbine rotor. It is easy to generalize this equation because there is no thrust extracted in the upwind flow. For any x and $z \leq 0$:

$$\int_{-\infty}^z \left(P\frac{dx}{dz}\right)_{S(x,z)} x dz = \frac{1}{2}\int_0^x \left(a^2 - v^2\right) x dx \tag{15}$$

where $S(x,z)$ is the streamsurface passing through (x,z) so that $BS = S(1,0)$. The second integral is evaluated at $z \in [-\infty, 0]$.

P_D in (12) can be evaluated in the standard manner by assuming that the unsteady Bernoulli equation is valid from immediately behind the rotor to the far-wake:

$$-\frac{2P_D}{\rho} = u^2 + v^2 + w^2 - u_\infty^2 - w_\infty^2 - \frac{2P_\infty}{\rho} - 2\lambda x_\infty w_\infty + 2\lambda x w \tag{16}$$

where the far-wake terms have the subscript "∞". The last two terms arise from the unsteady potential terms, evaluated by assuming rigid wake rotation (see appendix B of LW). Conveniently, these terms cancel due to conservation of angular momentum, yielding

$$-\frac{2P_D}{\rho} = u^2 + v^2 + w^2 - u_\infty^2 - w_\infty^2 - \frac{2P_\infty}{\rho}. \tag{17}$$

Combining (12) and (17) we get

$$\frac{T}{\pi\rho} = \int_0^1 \left(1 - u_\infty^2\right) x dx - \int_0^1 \left(\frac{2P_\infty}{\rho} - w^2 + w_\infty^2\right) x dx, \tag{18}$$

where w_∞ and P_∞ are evaluated at x_∞ in the wake, connected to x at the rotor by a mean streamsurface.

In the far-wake, the pressure and circumferential velocity are related by

$$\frac{dP_\infty/\rho}{dx} = \frac{w_\infty^2}{x}. \tag{19}$$

The relationship between the area integrals of P and w can be found using the technique introduced by McCutchen (1985) and rediscovered by Wood (2007): multiply both sides by x^2 and integrate, by parts for the left side. If $P_\infty x^2 \to 0$ as $x \downarrow 0$, and is zero at the edge of the far-wake, then

$$\int_0^{R_\infty} \frac{P_\infty}{\rho} x\,dx = -\frac{1}{2} \int_0^{R_\infty} w_\infty^2 x\,dx. \tag{20}$$

As pointed out by van Kuik (2018) in conjunction with his Equation (6.8), any swirl at the edge of the wake makes $P_\infty(x_\infty) \neq 0$. The present analysis can accommodate this behaviour but for the present we take the simpler path of assuming $P_\infty(x_\infty) = 0$. The main justification for this assumption is that we expect the magnitude of the swirl to become negligible everywhere at the edge of the wake at high λ. When $P_\infty(x_\infty) = 0$, Equation (18) reduces to

$$\frac{T}{\pi\rho} \approx \int_0^1 \left(1 - u_\infty^2\right) x\,dx + \int_0^1 w^2 x\,dx, \tag{21}$$

Defining the axial induction in the far wake as $a_\infty = 1 - u_\infty$, we obtain

$$\frac{T}{\pi\rho} \approx \int_0^1 a_\infty \left(2 - a_\infty\right) x\,dx + \int_0^1 w^2 x\,dx, \tag{22}$$

and the standard thrust equation is recovered if $a_\infty \approx 2a$ and $w^2 \approx 0$ which is typically the case at high λ but may not be generally correct. Note that (22) is accurate at $\lambda = 0$ where the first integral is negligible but $a_\infty \neq 2a$.

To recover the classical thrust equation, and to provide a comparison to the analyses of Sørensen (2016) and van Kuik (2018), we now move the downwind face of the CV to the far-wake and use Equation (20). This results in

$$\frac{T}{2\pi\rho} = \int_0^{R_\infty} a_\infty \left(1 - a_\infty\right) x\,dx - \int_0^{R_\infty} \frac{P_\infty}{\rho} x\,dx = \int_0^{R_\infty} a_\infty \left(1 - a_\infty\right) x\,dx + \frac{1}{2} \int_0^{R_\infty} w_\infty^2 x\,dx. \tag{23}$$

If we ignore the second integral in (18) and the integrals in (23) containing P and w, and assume a and a_∞ are constant with x, we again recover the conventional relation $a_\infty \approx 2a$ once the conservation of mass is invoked.

In considering the local equation for dT/dx in the next Section, it is useful to have the alternative form of (23) from the impulse analysis of LW. The direct application of LW's Equation (22):

$$\frac{T}{2\pi\rho} = \int_0^\infty \left(\tfrac{1}{2}w^2 + \lambda wx\right) x\,dx + \frac{1}{2} \int_0^\infty \left(v^2 - a^2\right) x\,dx. \tag{24}$$

together with $v = 0$ everywhere in the far-wake and $a_\infty = 0$ for $r > R_\infty$ gives

$$\frac{T}{2\pi\rho} = \int_0^{R_\infty} \left(\tfrac{1}{2}w_\infty^2 + \lambda w_\infty x\right) x\,dx - \frac{1}{2} \int_0^{R_\infty} a_\infty^2 x\,dx. \tag{25}$$

Note that (24) holds anywhere behind the rotor, i.e. for $z > 0$ with the second integral approaching zero as $z \downarrow +0$.

The results for the far-wake can be used to estimate the conventional thrust when $\lambda = 0$ and the expansion is negligible by application to S_D. Equation (20) will then be approximately valid for a and P_D replacing a_∞ and P_∞, and comparison with (1) shows that the momentum flux term $2a(1-a)$ will be negligible. In other words, the thrust on a stationary disc occurs predominately through the pressure on its back face associated with w.

3 Local thrust in expanding flow

Having considered the thrust for the complete rotor, we now consider the "local" contribution at radius x. We continue to do this for a circumferentially-uniform disc. It is easy to show that the local form of (12),

$$\frac{1}{\pi\rho}\frac{dT}{dx} = \left[2a(1-a) - \frac{2P_D}{\rho} + a^2 - v^2\right]x, \tag{26}$$

is exact for a circumferentially-uniform disc in expanding flow. This can be done in at least two ways. First, using Equation (7) and simple manipulation, the bracketed terms become

$$1 - u^2 - v^2 - \frac{2P_D}{\rho} = \frac{2\Delta P}{\rho} \tag{27}$$

and the pressure difference across the annulus containing the blade elements must give the exact thrust by assumption #4. Secondly, starting from Equation (15) it is easy to prove that $a^2 - v^2$ in (26) accounts for the difference in pressure acting on the top and bottom of the expanding annular streamtube that intersects the blade elements.

We now consider the consequences of the exact Equation (26) for the far-wake. If the w and P_∞ terms in (17) are negligible at high λ, the bracketed term in (26) becomes

$$2a(1-a) - \frac{2P_D}{\rho} + a^2 - v^2 \approx 1 - u_\infty^2. \tag{28}$$

The exactness of the local form of (23) is not easy to establish in general because all three velocity components can be important in the wake and the total pressure is not constant. This is the first reason we based our analysis on the CVs shown in figure 1 rather than one extending to the far-wake. We note, however, that there is no interchange between pressure on BS and axial momentum in the flow outside the far-wake where $v^2 = a^2 = 0$. In other words, the interchange is completed before the far-wake is reached. This is the second reason we used the CVs in figure 1. The local form of (23) will have a term corresponding to the bracketed term in (26) of $2u(1-u_\infty)$. Combining with (28), we retrieve the standard result that $u = (1+u_\infty)/2$ or $a_\infty = 2a$ which can be accurate only at high λ; note that the discussion immediately below (22) shows the result does not hold at $\lambda = 0$. Further, from (7)

$$\frac{2P_U}{\rho} = 1 - u^2 - v^2 = 2a(1-a) + a^2 - v^2. \tag{29}$$

If Equation (6) is valid, then (26) becomes

$$-\frac{2P_D}{\rho} \approx 2a(1-a) - a^2 + v^2. \tag{30}$$

8

205   for $x \leq 1$.

The preceding analysis shows that $P_U \neq -P_D$ in general, in contrast to the familiar results of one-dimensional momentum theory. $P_U = -P_D$ would require $a = v$, which cannot hold everywhere for several reasons. First, $v \to 0$ as $x \downarrow 0$ whereas there is no similar constraint on a. Secondly, we argued above that the flow outside the wake has an axial momentum deficit so $a \geq 0$ but not necessarily equal to v for $x > 1$. Equation (2) would then be violated if $a = v$ for $x \leq 1$. Thirdly, van Kuik (2018)

210   Section 5.4.4 points out that there is no theoretical requirement that $P_U = -P_D$. They are unlikely, however, to differ greatly in general. This suggests $v \to a$ as $x \to 1$, as argued by LW, and shown by the model calculations of van Kuik (2020), who found also that v was significantly larger than a outside the wake until at least $x \approx 1.2$. If $a > v$ over most of the rotor, then the positive $a^2 - v^2$ in (26) corresponds to a positive pressure exerted by the external flow on the wake.

A more definite statement about P_U and P_D can be made for stationary rotors ($\lambda = 0$) following the last paragraph of the

215   previous Section. It is shown there that a is negligible at $\lambda = 0$ so that $P_U \approx 0$ and P_D is associated with w behind the rotor. The inequality reduces as λ increases but is always present because of nonzero $a^2 - v^2$.

We now consider the far-wake in more detail to determine the vortex pitch and its relation to a_∞ which are required in the next section. Equation (19) requires $P_\infty/\rho = -w_\infty^2/2$ when $w_\infty \sim 1/x_\infty$. We assume that at sufficiently high λ, the flow downwind of the rotor approximates a Joukowsky wake with the hub vortex lying along the axis of rotation and the tip vortices

220   at radius R_∞ in the far-wake, with no vorticity in between. The main justification for this assumption comes from Equation (1). When $\lambda = 0$, the first term implies that the bound vorticity, Γ, cannot be constant; Wood (2015) showed that $\Gamma \sim x^2$. At high λ however, the first term becomes negligible in comparison to the second for most x. The simplest wake for which the thrust remains bounded on a turbine with N blades occurs when $N\Gamma\lambda \sim \lambda w x$ is constant in x and λ; this is the Joukowsky wake in which Assumption #7 of Section 1 becomes irrelevant to the flow between the tip and hub vortices. Further, the tip

225   vortices now separate the wake and the external flow which may have very different velocities. The vortex velocity should then be the average of these two and the vortex lines need not align with the wake streamlines.

Outside the hub vortex core of a Joukowsky wake, $w_\infty \sim 1/x_\infty$ and, as pointed out by Sørensen (2016), the total pressure is constant for all streamsurfaces. In addition, independence will hold in the sense that the integrands in (23) and (25) must be equal. Thus

230
$$\frac{1}{2}w_\infty^2 + \lambda w_\infty x - \frac{1}{2}a_\infty^2 = a_\infty\left(1 - a_\infty\right) + \frac{1}{2}w_\infty^2 \tag{31}$$

without making any assumption about the relationship between a and a_∞. p_∞, the constant pitch of the constant radius tip vortices, is related to the velocities by the equivalent of Equation (4): $p_\infty/x_\infty = w_\infty/a_\infty$. Equation (31) can be rewritten as

$$p_\infty = \frac{1 - a_\infty/2}{\lambda}. \tag{32}$$

In the next section, λ will be calculated using Equation (32) for a given p_∞ and the corresponding calculated value of a_∞.

235   Equation (32) is the high$-\lambda$ equivalent of Equation (22) of Okulov & Sørensen (2008) for vortex pitch provided the convection velocity of the vortex—w in their notation but w_v here—is equal to $a_\infty/2$. Table 1 of Wood & Okulov (2017) shows that $w_v \to a$ for ideal Betz-Goldstein rotors as $\lambda \to \infty$ and so (32) is recovered since $a_\infty \to 2a$ in the same limit. Another way to

view this result is that the axial velocity in the Joukowsky far-wake is constant and equal to $1 - a_\infty$ outside the vortex cores, so the tip vortices must travel downwind at a velocity of $1 - a_\infty/2$ to be force-free.

240 The KH equations for a doubly-infinite helical vortex of constant radius and pitch, lead to

$$a_\infty = N\Gamma/(2\pi p_\infty). \tag{33}$$

If we ignore wake expansion, then $a \approx N\Gamma/(4\pi p)$ for the singly-infinite near-wake, and if $p_\infty \approx p$, then $a_\infty \approx 2a$. This result suggests the strategy for the next Section, where we analyze the flow associated with *expanding* tip vortices by assuming they have constant pitch everywhere. This allows a semi-analytic determination of their influence on the flow through the rotor.

245 In other words, we relax one of the limitations of the KH equations, that of constant radius, which is necessary, but keep the limitation on p, which, hopefully, leads to results of sufficient generality.

4 The expanding Joukowsky wake with constant pitch

We assume p remains constant and use the results of the previous section and the Biot-Savart law to investigate the flow immediately behind the rotor and determine the thrust and power coefficients. The circumferentially-averaged velocities are

250 due entirely to the trailing vorticity: w is due to the hub vortex only, whereas u and v result from the expanding tip vortices only.

4.1 Biot-Savart analysis of expanding tip vortices

Without loss of generality, let the lifting line representing one blade lie instantaneously along the $x-$axis in Figure 1 and consider the tip vortex beginning at $(1,0,0)$. We now determine the velocities induced at a point $(x,\theta,0)$ in polar co-ordinates or

255 $(x\cos\theta, x\sin\theta, 0)$ in Cartesian co-ordinates for constant p. A point on the vortex is $(t(\beta), \beta, p\beta)$ or $(t(\beta)\cos\beta, t(\beta)\sin\beta, p\beta)$ where radius t is a monotonically increasing function of the vortex angle β that asymptotes to the far-wake radius. Thus $1 \le t \le R_\infty$, and from here on, the dependence of t on β will be understood. An increment dl along the vortex is given by

$$dl = (-t\sin\beta + \frac{dt}{d\beta}\cos\beta, t\cos\beta + \frac{dt}{d\beta}\sin\beta, p)d\beta \tag{34}$$

and the distance d from the point to the vortex is

260 $$d = (x\cos\theta - t\cos\beta, x\sin\theta - t\sin\beta, -p\beta) \tag{35}$$

so that

$$d^2 = x^2 + t^2 - 2xt\cos(\beta - \theta) + p^2\beta^2 \tag{36}$$

which is an even function of β and θ. A straightforward application of the Biot-Savart law yields the three velocities associated with the trailing tip vortex as

265 $$\big(v(x,\theta), w(x,\theta), a(x,\theta)\big) = \frac{\Gamma}{4\pi}\left(I_v, I_w, I_a\right) = \frac{\Gamma}{4\pi}\int\limits_0^\infty \frac{\big(i_v(x,\theta), i_w(x,\theta), i_a(x,\theta)\big)}{d^3}d\beta \tag{37}$$

10

where Γ is the vortex strength,

$$i_v(x,\theta) = -p\left[t\beta\cos(\beta-\theta) + \left(t - \beta\frac{dt}{d\beta}\right)\sin(\beta-\theta)\right], \tag{38}$$

$$i_w(x,\theta) = p\left[x + \left(\beta\frac{dt}{d\beta} - t\right)\cos(\beta-\theta) - \beta t\sin(\beta-\theta)\right], \quad \text{and} \tag{39}$$

$$i_a(x,\theta) = t^2 - xt\cos(\beta-\theta) - x\frac{dt}{d\beta}\sin(\beta-\theta). \tag{40}$$

In forming the circumferential averages by integrating over $0 \leq \theta \leq 2\pi$, all the $\sin(\beta-\theta)$ terms will vanish as they are odd in θ. The linearity of inviscid flow leads to equal contributions to the averaged (u, w, a) from the N identical and equi-spaced trailing vortices.

The simplest calculation of i_a is for $x = 0$ for which the circumferential average $a(0) = a(0, \theta)$, and

$$a(0) = \frac{N\Gamma}{4\pi}\int_0^\infty \frac{t^2}{(t^2 + p^2\beta^2)^{3/2}}d\beta = \frac{N\Gamma}{4\pi p}\int_0^\infty \frac{t^2}{(t^2 + z^2)^{3/2}}dz = \frac{N\Gamma}{4\pi p}\int_0^\infty i_a(0)dz = \frac{N\Gamma}{4\pi}I_a(0). \tag{41}$$

I_a is, clearly, dependent only on the geometry of the tip vortices. For an expanding wake with constant p, Equation (4) will underestimate a as $I_a(x) \geq I_a(0) \geq 1/p$ when t is not constant. If p varied with β, then $p\beta$ in Equation (36) would be replaced by $\int p\,d\beta$ and the direct relation between $\partial/\partial z$ and $(1/p)d/d\beta$ would be lost. It is likely that an analytic expression for the integrands in (37) would not be possible.

Performing the θ−integration of (40) using Mathematica gives

$$i_v(x) = \frac{p\beta}{\pi x\sqrt{p^2\beta^2 + (x+t)^2}}\left[\left(1 + \frac{m}{2}\right)\mathrm{E}(m_p) - \mathrm{K}(m_p)\right], \quad \text{and} \tag{42}$$

$$i_a(x) = \frac{-1}{\pi\sqrt{p^2\beta^2 + (x+t)^2}}\left[\left(1 + \frac{m}{2} - \frac{mt}{2r}\right)\mathrm{E}(m_p) - \mathrm{K}(m_p)\right], \tag{43}$$

where $m = 4xt/(p^2\beta^2 + (x-t)^2)$. E(.) and K(.) are the complete elliptic integrals of the second and first kind, respectively, whose argument, $m_p = m/(1+m)$. Thus v and a can be obtained by integrating (41) along the trajectory of the tip vortex, $t(\beta)$ for $0 \leq \beta \leq \infty$. This must, in general, be done numerically, but several checks are possible. In describing these, we continue to use the notation $I = \int i\,d\beta$ and identify the limits to the integral if they differ from $(0, \infty)$.

If t remains constant at 1, say, and the integration is over $-\infty \leq \beta \leq \infty$, that is for a doubly-infinite vortex or vortices of constant radius and pitch, then $I_v(-\infty, \infty) = 0$ for any x, and

$$I_a(-\infty, \infty) = 2/p, \quad \text{for } x < 1,$$
$$= 1/p, \quad \text{for } x = 1, \quad \text{and} \tag{44}$$
$$= 0, \quad \text{otherwise.}$$

The interior and exterior solutions in (44) are consequences of the KH equations, derived from the velocity potential. All results in (44) follow from Equation (37). Using *NIntegrate* in Mathematica and Matlab's *integral*, these results were reproduced to

six significant figures for a similar range of x to that used in the main text and limits of $\pm 1000\pi$ on the integration. For a singly-infinite helix, the values of I_a for $z = 0$ when $\beta = 0$, are half those in (44). These were reproduced numerically to the same accuracy. I_v is not available from the KH equations for this case.

As with any Biot-Savart analysis, the behaviour of Equations (42) and (43) as $x \to t(0) = 1$ must be considered. As $m_p \to 1$, $E(m_p) \sim 1$, Formula (19.6.1) of DLMF (2021), and $K(m_p) \sim \log(16/m_p')/2$ where $m_p' + m_p = 1$, Formula (17.3.26) of Abramowitz & Stegun (1964). The leading terms in (42) and (43) become

$$i_v(x) \sim p\beta(p^2\beta^2 + x^2 + t^2)/\sqrt{p^2\beta^2 + (x+t)^2}/x/\left(p^2\beta^2 + (x-t)^2\right), \quad \text{and} \tag{45}$$

$$i_a(x) \sim -(p^2\beta^2 + x^2 - t^2)/\sqrt{p^2\beta^2 + (x+t)^2}/\left(p^2\beta^2 + (x-t)^2\right). \tag{46}$$

showing that a logarithmic singularity occurs in i_a despite it being the integrand for the circumferentially-averaged axial velocity. This is a stronger singularity than that in Chattot's (2020) perturbation analysis of the flow near the edge of the rotor, which assumes a vortex cylinder wake. There is no logarithmic singularity in i_v, but the slope $di_v/d\beta$ increases without bound as $\beta \to 0$. These behaviours could be mitigated by using the well-known "cut-off" modification to the limits of the Biot-Savart integrals as was done for helical vortices by Ricca (1994), see also Section 11.2 of Saffman (1992). There is, however, a simpler, heuristic alternative. The upper limit on $a(x)$ as $x \to 1$ is taken to be a_∞. A partial justification for this tactic comes from the wind tunnel measurements of a model wind turbine by Krogstad & Adaramola (2012). Their Figure 9(c) shows that at $\lambda = 9.51$, $a \approx 0$ at small x but rises to the extraordinary value of around 0.8 at $x = 1$. Thus $I_a \le 2/p$ was enforced in the calculations described in the main text. Whenever this was done, I_v was assumed equal to the maximum value below the limit on I_a.

The numerical evaluation of I_a and I_v can be improved by considering the asymptotic behaviour of i_a and i_v for large β which corresponds to small m and m_p. The leading terms are simple functions of β, allowing the infinite integrals to be approximated. For I_v, we have

$$I_v(x) \approx I_v(x, \widehat{\beta}) + R_v(\widehat{\beta}) \tag{47}$$

where the first term was obtained numerically over $\beta = [0, \widehat{\beta}]$ and the remainder, $R_v(\widehat{\beta})$, is an approximation to the integral over $\beta = [\widehat{\beta}, \infty]$. $R_v(\widehat{\beta})$ is

$$R_v(\widehat{\beta}) = xR_\infty^2/(2\widehat{\beta}^3 p^4). \tag{48}$$

The remainder for I_a is independent of x:

$$R_a(\widehat{\beta}) = R_\infty^2/(2\widehat{\beta}^2 p^3). \tag{49}$$

This result also follows from (41) when $z >> R_\infty$.

It was found that $\widehat{\beta} = 200\pi$ was sufficient to ensure six-figure accuracy of the integrals over the range of x considered below. I_v converged faster than I_a, reaching 99% of the final value by $\beta = 2\pi$ for any x.

The Biot-Savart integrands in Equation (43) are plotted in Figures 3 and 2 for x close to the blade tip, in terms of axial distance $z = p\beta$ where β is the vortex angle starting from zero at the rotor. The figures also show the small$-\beta$ asymptotes in Equations (45) and (46), and the large$-\beta$ remainders defined in (48) and (49). If the tip vortex radius t remains at 1, Equation (44) gives $I_a = 1/p$ for any x, and the conventional momentum equation (6) remains valid. We assume that $1/p$ is the minimum value of I_a, and, as explained in the Appendix, we impose $a \leq a_\infty$ so that $1/p \leq I_a \leq 2/p$. For maximum power, the familiar derivation of the Betz-Joukowsky limit suggests $R_\infty^2 \approx 2$ so we investigate R_∞ around that value. Note, however, the use of Equation (6) to derive this limit means that it is applicable only to a wake that expands either very slowly, as explained above, or very rapidly to $t = \sqrt{2}$, as $I_a = 1/p$ for any constant t. We will show that generic wind turbine wakes at high λ expand at a rate that is intermediate between these extremes which causes Equation (6) to be inaccurate. There is no direct maximization of power output in the following analysis. Instead, the wake model is constrained as we now describe.

Solving (37) for I_a and I_v, requires p and the tip vortex trajectory. We used the very simple form:

$$t = R_\infty - (R_\infty - 1)\exp(-k\beta) \tag{50}$$

which satisfies three necessary conditions: $t = 1$ when $\beta = 0$, $t \to R_\infty$ for large β, and t and its derivatives are continuous. The fourth condition is that k must satisfy the reduced version of Equation (2):

$$\int_0^\infty \left(I_v^2 - I_a^2\right) x \, dx = 0. \tag{51}$$

This integral will be called the "Expansion Integral". It uniquely fixes k for any choice of R_∞^2 and p. I_a and I_v were obtained using the Matlab function *integral* over $\beta = [0, 200\pi]$ to an absolute tolerance of 10^{-6}. The remainders, Equations (48) and (49), were then added. The expansion integral, and the mass flux integral described below, were found by trapezoidal integration using the points shown in Figure 4. The expansion integral is large for small k as v is (not obviously) maximized when there is very little vortex expansion near the rotor.

The mass flux through the rotor, using (33) to remove $N\Gamma$, determines a_∞:

$$1 - a_\infty p \int_0^1 I_a x \, dx = (1 - a_\infty) R_\infty^2. \tag{52}$$

Equation (32) then yields λ. A number of possible methods were considered for solving the integral in (52). $i_a(x, \theta)$ can be written as

$$i_a(x, \theta) = \frac{d}{dx}\left(\frac{x}{d}\right) - \frac{p^2 \beta^2}{d^3} \tag{53}$$

which allows an analytic integration of $i_a(x, \theta)x$ in x. The resulting expression is complicated and probably requires numerical integration in θ and β to obtain the mass flux. Further, the integrand is singular at a point that varies with θ and β. The simpler alternative of numerical integration of $I_a x$ was used.
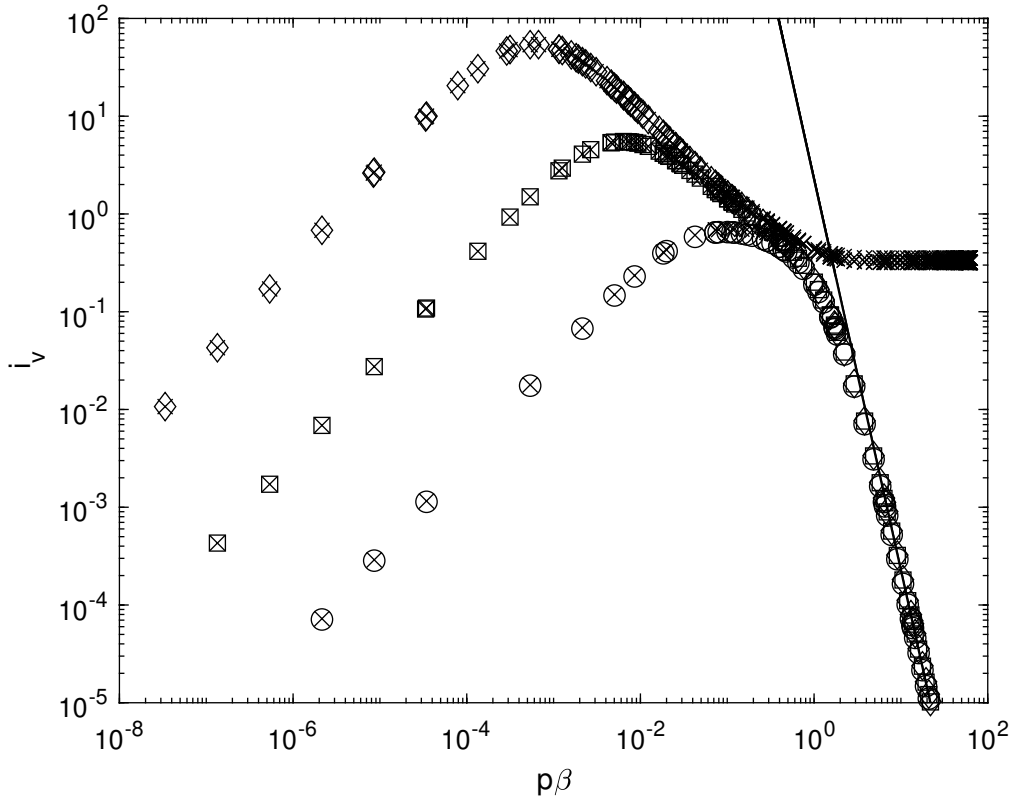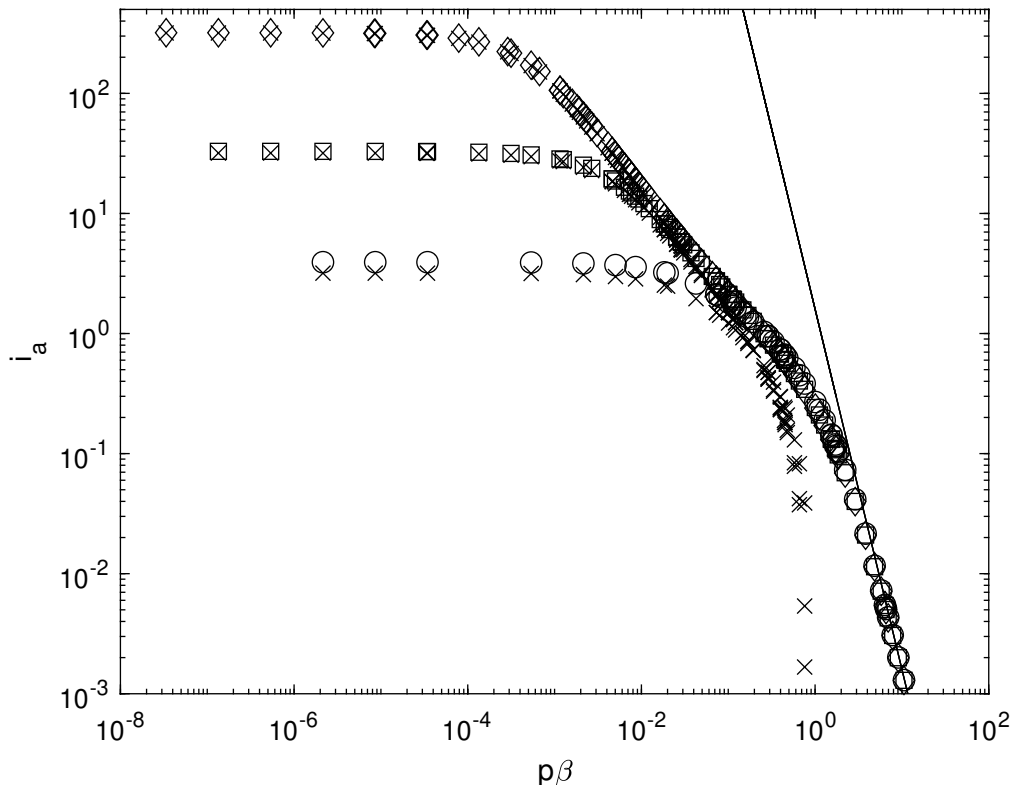
Figure 2. Integrand, i_v, for $p = 0.1$, $R_\infty^2 = 1.597$. $\circ$, $x = 0.9$; $\square$, $x = 0.99$,; and $\diamond$, $x = 0.999$ from Equation (42). i_a increases with x. $\times$ is the integrand in (45). For clarity, only every second data point is plotted. The solid line shows the remainders from (48). The differences with varying x are within the thickness of the line.

To find the unique R_∞^2, we impose the further condition that k must match the slope of the vortex surface at the rotor. Then k in Equation (50) equals $k_\star$, given by

$$\frac{dt}{dz}(\beta = 0) = \frac{v(x = 1)}{1 - a(x = 1)} = (R_\infty - 1)\frac{k_*}{p}. \tag{54}$$

4.2 Results

355   The results in Table 1 were obtained using the Matlab routine *patternsearch* to minimize the single objective function that combined the magnitude of the expansion integral and $|k - k_*|$. This, surprisingly, occurred at a constant value of k_*/p, implying that the vortex expansion to the far-wake radius happens over a fixed distance and the surface containing the vortices has the same shape, independent of p or λ.

Figure 3. Integrand, i_a, for $p = 0.1, R_\infty^2 = 1.597$. $\circ, x = 0.9$; $\square, x = 0.99$,; and $\diamond$, $x = 0.999$ from Equation (43). i_a increases with x. $\times$ is the integrand in (46). For clarity, only every second data point is plotted. The solid line shows the remainders from (49).

p	R_∞^2	k_*	λ	a_∞	C_P	C_T	C_T'	ΔC_T
0.10	1.597	0.4947	7.13	0.574	0.557	0.819	0.866	0.067
0.05	1.592	0.2482	14.28	0.572	0.556	0.817	0.864	0.067

Table 1. Results for the expanding Joukowsky wake with constant pitch

Figures 2 and 3 show the integrands i_v and i_a are large in the vicinity of the rotor. Their size implies that the simple assumed
360   shape of the tip vortex trajectory, Equation (50), is reasonable, and that adding a term or terms, say, to control the approach to the far-wake would not change the analysis significantly.

Figure 4 shows a and v at the rotor for the cases in Table 1 are independent of p. $a(0) = 0.296$, that is less than the Betz-Joukowsky value of 1/3, and $v(0) = 0$ as it must. The "non-expansion" results for v and $a = 1/3$ within the wake, are shown as solid lines. Note that $a = 0$ for $x > 1$ but v is very large near the edge of the rotor and it is clear that the expansion integral
365   cannot be satisfied. The limit $a \leq a_\infty$ was applied near the blade tip for the expanding wake, where v has increased to be nearly
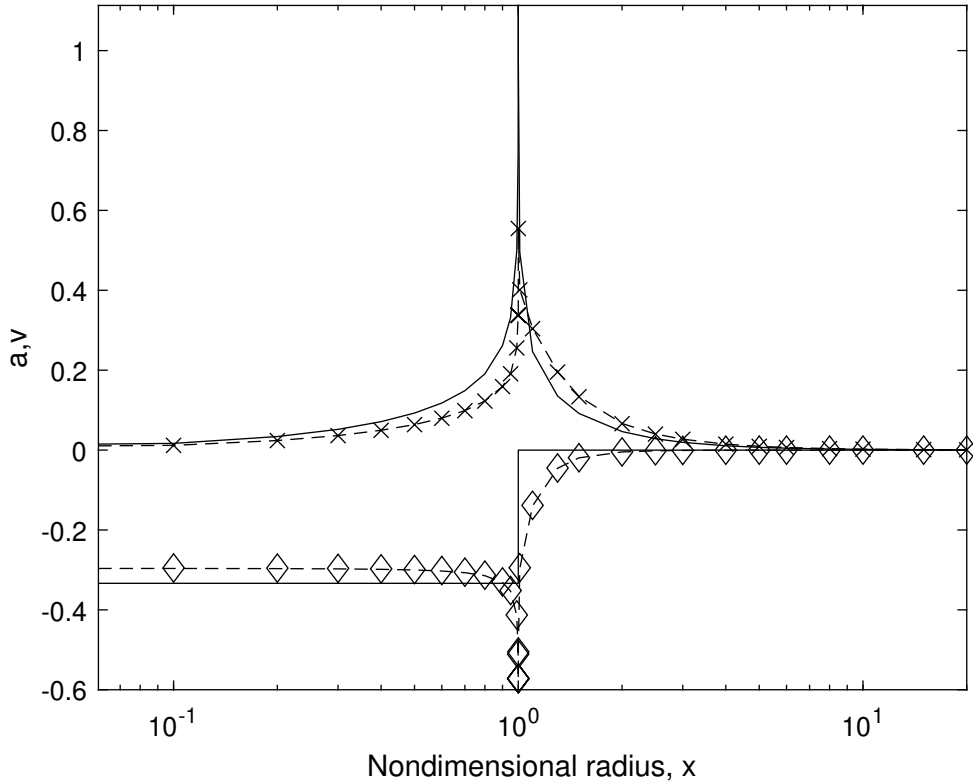
Figure 4. Axial induction, a, and radial velocity, v, for the conditions in Table 1. $p = 0.05 : a, \diamond; v, \times$. The corresponding results p=0.10 are shown as dashed lines. Note that $-a$ is shown to make it distinct from v. The solid lines show a and v for "no expansion", i.e. $k = 0$, $R_\infty = 2$. The $x-$axis is logarithmic.

equal, but smaller than a. Outside the wake, $v > a$ and takes till $x = 3$ to fall to 0.03. Similar shaped distributions of a and v for a Joukowsky wake are shown in Figure 5 of van Kuik (2020), who also found that Equation (2) was satisfied in his low$-\lambda$ simulations.

The final calculations were for C_T from (1) with w^2 ignored because λ is large:

370 $$C_T \approx N\Gamma\lambda/\pi \approx 2a_\infty p\lambda \approx 2a_\infty(1 - a_\infty/2) \tag{55}$$

using (32) and (33). We note that (1) makes the high$-\lambda$ blade element thrust constant across the rotor whereas the familiar form involving the axial velocity equation in (6) requires a significant variation near the tip. From conservation of angular momentum, and finding the power as the product of torque and angular velocity:

$$C_P \approx C_T(1 - a_\infty)R_\infty^2 \tag{56}$$

16
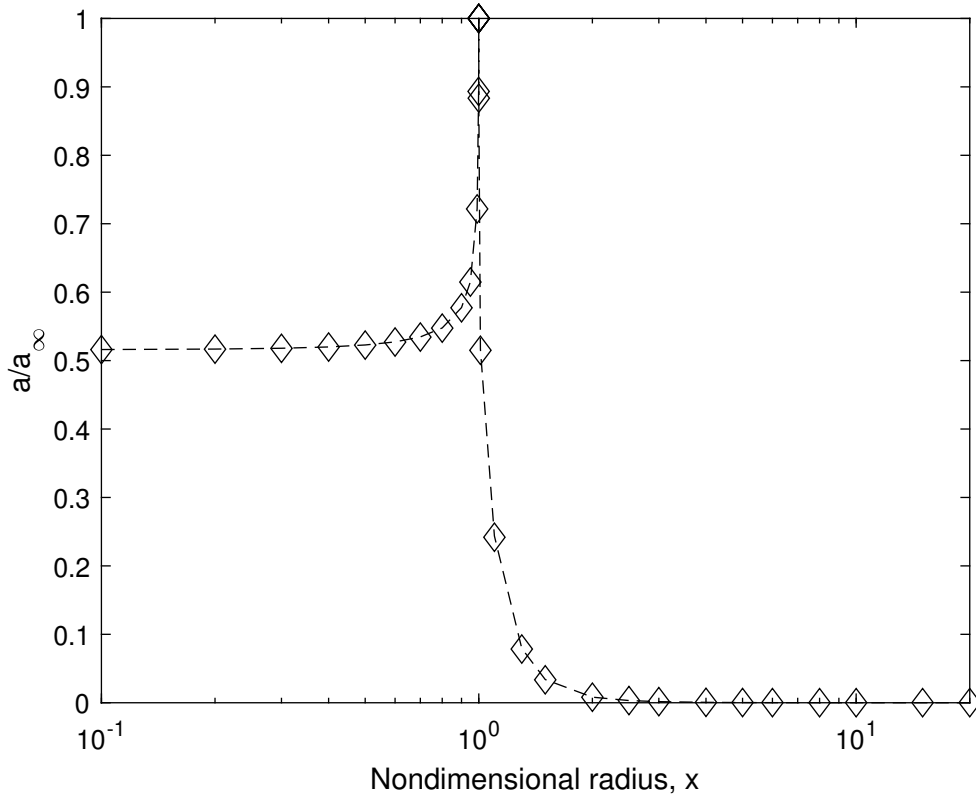
Figure 5. Ratio of axial induction at the rotor, a, to value in the far-wake, a_∞. $p = 0.05 : \circ.p = 0.10$, solid line. Note that the $x-$axis is logarithmic.

375 so the power extraction also decreases significantly near the tip. Equation (56) and the third component of (55) also hold for the conventional analysis that leads to the Betz-Joukowsky limit.

Table 1 shows the biggest change from the familiar Betz-Joukowsky wake is the 20% reduction in R_∞^2 which occurs because $a > a_\infty/2$ for much of the rotor, Figure 4. In other words, more of the expansion occurs upwind of the rotor. In contrast, the maximum C_P is reduced by only 6% to 0.557 and the mass flux is increased by 2%. The second last column in Table 1, gives 380 C_T', the conventional thrust coefficient evaluated from Equation (6):

$$C_T' = 8 \int_0^1 a(1-a)x dx. \tag{57}$$

As shown by $\Delta C_T = C'_T - C_T$, the conventional equation over-estimates the thrust by around 5%. From Equations (29) and (30), we get the integrated asymmetry of the disc pressure distribution at high λ as

$$\int_0^1 \left(\frac{P_U}{\rho} + \frac{P_D}{\rho} \right) x dx \approx \int_0^1 (a^2 - v^2) x dx. \tag{58}$$

From the data in Table 1, the integral of δ_P is 0.087, so the magnitude of P_D is generally significantly less than that of P_U. It was shown in the previous section that the pressure integrals are equal in magnitude in the minimally-expanding wake when $\lambda = 0$ but the analysis in this section shows divergence in the expanding Joukowsky wake at high λ.

5 Discussion

The pressure in the expanding flow ahead of a wind turbine contributes to the axial force on the rotor and a momentum deficit in the flow outside the rotor. Researchers have been aware of these two effects for many years but the present analysis provides the first quantitative determination of them in Equations (14) and (15) derived by approximating the rotor as an actuator disc. The effects on the disc in integral and incremental form depend on $a^2 - v^2$ where v is the normalized radial velocity and a is the usual axial induction factor. Further, $v^2 - a^2$ can be used to quantify the external flow disturbed by the wind turbine and so may be useful to the study of multiple rotors in close proximity, as analyzed by, for example, Branlard and Meyer Forsting (2020) . One way to do this is by defining I_E as

$$I_E = \int_{x_{BS}}^{\infty} \left(v^2 - a^2 \right) x dx = - \int_0^{x_{BS}} \left(v^2 - a^2 \right) x dx \tag{59}$$

where x_{BS} is the radius of BS at any $z \leq 0$. The last integral is a consequence of Equation (2) being valid for S_U lying anywhere in the upwind flow. I_E must be zero in the undisturbed upwind flow. It then increases to its maximum value at the rotor according to the present analysis. I_E then decreases in the wake to be zero in the far-wake. In other words, the perturbation to the external flow is complete by the time the far-wake is reached. Note that the second equality in (59) does not hold in the wake.

The impulse analysis of Limacher & Wood (2020) (LW) showed that the Kutta-Joukowsky (KJ) equations for rotor thrust, Equation (1), and for the blade element contributions to the thrust, (3), are exact in the presence of wake expansion, where "exact" means using no more assumptions or approximations than the eight listed in the Introduction. The KJ equations, containing only the circumferential velocity and tip speed ratio, are not equivalent to the conventional equation involving only the axial velocity, when the flow expands. This is the outcome of the analysis in Section 4 where an expanding Joukowsky wake comprising tip and hub vortices of constant pitch was analyzed. The conventional thrust equation is altered by around 5-10%, depending on the trajectory of the tip vortices because the geometrical relation in Equation (4) is modified by the expansion.

The first three sections of the paper used only the standard form of control volume (CV) analysis for axial momentum to determine the thrust of the rotor and the incremental thrust of the blade elements comprising the rotor. To clarify the effects of expansion, most analysis in this paper used CVs with downwind faces in the immediate vicinity of the rotor, as opposed

to their common placement in the far-wake. The rotor and the flow are assumed to be circumferentially-uniform. We argued in the Introduction that the impulse analysis provides a simple and novel perspective on the role of the pressure. The thrust equations derived in Section 3 for the rotor, and in Section 4 for the local flow at any radius, contain the pressure acting on the downwind face of the actuator disk, which must be removed to make the equations suitable for actual blade analysis. Removal can be done accurately only for very low tip speed ratios where the expansion and its effects, are small.

To the rotor thrust, the pressure along the bounding streamsurface adds a term containing the integral of $a^2 - v^2$ over the rotor. This integral is equal and opposite the integral for the flow outside the wake so there is no net contribution to the thrust determined using the CVs shown in Figure 1. Unsurprisingly, the corresponding term in the local thrust equation at any x also contains $a^2 - v^2$. It follows that the conventional local thrust equation implies $a \approx v$ but a^2 is generally larger than v^2 over the rotor, but more precise estimates of v do not appear to be possible. $a^2 > v^2$ implies that the pressure adds to the rotor thrust and is associated with a momentum deficit in the external flow. The common derivation of the axial momentum equation which leads to the Betz-Joukowsky limit, ignores the interaction of pressure and external momentum and then ignores the radial velocity in relating the pressure at the rear of the disc to the far-wake. These errors cancel, so the main failing of the conventional equation is the breakdown of the relation $a_\infty = 2a$ when expansion is significant. The previous Section suggests this breakdown is due to the expanding tip vortices at high λ in the Joukowsky wake. At the rotor, the slope of the streamsurface containing the tip vortices is $53°$ for maximum power extraction, Table 1, so their trajectory is intermediate between very slow and very rapid expansion, either of which would require $a_\infty = 2a$. This analysis used Equation (32) for the pitch of the tip vortex, found by moving the CV outlet to the far-wake and using LW's impulse equation for thrust. We note that van Kuik (2020) estimated the streamsurface angle at the rotor edge to be $46°$ which is close to the present value. The effect of the expansion on a was constrained so that $a \leq a_\infty$ as an alternative to using a cut-off in the Biot-Savart integral. Figure 4 shows that a increased with radius to reach a_∞ in the streamtube bounded by the tip vortex, suggesting a very substantial effect of expansion. Qualitatively, this large value of a is in agreement with the wind tunnel measurements of Krogstad & Adaramola (2012) who found that a increased cross the rotor to reach 0.8 at the tip at high λ.

Including v in the axial momentum equation effectively adds an extra unknown to the conservation equations that may render them useless unless another equation for u, v or w could be derived. Further, high v may cause significant alterations to the lift and drag of the blade elements near the tip. To our knowledge, radial velocity effects on airfoil lift and drag have not been studied in the context of blade element theory.

The role of the radial velocity and flow expansion is probably more complicated in rotors with a limited number of blades than the actuator discs considered here. Eriksen & Krogstad (2017) measured u, v, and w immediately behind the rotor of a model three-bladed turbine out to a radius 20% larger than the blade tip radius. They used phase-locked averaging to obtain the flowfield as seen by an observer rotating with the blades. Significant phase variations occurred in a and v showing that the averages a^2 and v^2 over a blade revolution could be large even if the mean values of a and v are small. Nevertheless, the magnitude of both a and v was largest near the angular location of the blades, suggesting that the issues with radial deflection will occur in real turbines. We hope that these comments, and the present analysis, will inspire further measurements to be made far enough outside the wake to help clarify the role of flow expansion and the disturbances to the external flow.

6 Conclusion

This analysis started from the impulse-derived Kutta-Jukowsky equation for wind turbine thrust which does not involve the axial velocity. The equation is valid for any amount of expansion in the upwind flow and the wake and any distribution of bound circulation on the rotor. We were able to:

- Demonstrate the conventional thrust equation containing the axial velocity can be correct only when the tip speed ratio is large.

- Derive an exact expression for the effects of flow expansion on the conventional momentum equation. This involves the axial induction factor and the radial velocity.

- Apply the conventional and impulse thrust equations in the far-wake to give the pitch of the tip vortices in the Joukowsky wake in terms of the tip speed ratio and the far-wake induction.

- Find a semi-analytic solution of the Biot-Savart law for the induced velocities at the rotor by assuming the tip vortex had constant pitch. The axial velocity near the rotor tip approached the far-wake value, but was prevented from exceeding it as an alternative to using the familiar cut-off in the Biot-savart integrals. The increase in the rotor value contradicts the familiar relation that the axial induction factor everywhere at the rotor is half that of the far-wake.

- Derive in Section 5 the following results from the model of constant pitch, expanding tip vortices.

  1. The angle of the tip vortex surface to the wind direction was $53°$ for maximum power production, independently of the tip speed ratio and vortex pitch.

  2. Because it is neither very small nor very large, this expansion leads to an error of around 6% in the conventional thrust equation which would be accurate for both extreme expansions.

  3. The resulting wake expands less than the familiar Betz-Jukowsky wake. For two pitch values corresponding to tip speed ratios of 7 and 14, the far-wake area was 1.59 times the rotor area.

  4. Find the reduction in the rotor power and thrust due to expansion. The maximum power coefficient and corresponding thrust coefficient were 6% less than the values given by the Betz-Joukowsky limit.

  5. Quantify the influence of the expansion on the flow outside the rotor. For example, the radial velocity at three rotor radii is still 3% of the wind speed when the rotor is producing maximum power. The axial induction factor decays to zero more rapidly than the radial velocity as radius.

References

Abramowitz, M., Stegun, I. A. (Eds.). Handbook of mathematical functions with formulas, graphs, and mathematical tables (Vol. 55). US Government printing office, 1964.

Branlard, E., Meyer Forsting, A. R. (2020). Assessing the blockage effect of wind turbines and wind farms using an analytical vortex model. Wind Energy, 23, 2068-2086.

Burton, T., Jenkins, N., Sharpe, D.,& Bossanyi, E. Wind Energy Handbook. John Wiley & Sons, 2011.

Chattot, J. J.: On the Edge Singularity of the Actuator Disk Model. Journal of Solar Energy Engineering, 143(1), 2020.

NIST Digital Library of Mathematical Functions. http://dlmf.nist.gov/, Release 1.1.1 of 2021-03-15. F. W. J. Olver, A. B. Olde Daalhuis, D. W. Lozier, B. I. Schneider, R. F. Boisvert, C. W. Clark, B. R. Miller, B. V. Saunders, H. S. Cohl, and M. A. McClain, eds.

Eriksen, P. E., Krogstad, P. Å.: An experimental study of the wake of a model wind turbine using phase-averaging. International Journal of Heat and Fluid Flow, 67, 52-62, 2017.

Glauert, H.: Airplane propellers. In Aerodynamic theory (pp. 169-360). Springer, Berlin, Heidelberg, 1935.

Goldstein, S.: On the vortex theory of screw propellers. Proceedings of the Royal Society of London. Series A, 123(792), 440-465, 1929.

Goorjian, P.M.: An invalid equation in the general momentum theory of the actuator disc. AIAA Journal, 10(4): 543-544, 1972.

Hansen, M. O.: Aerodynamics of Wind Turbines. Routledge, 2015.

Hardin, J. C.: The velocity field induced by a helical vortex filament, Physics of Fluids, 25, 1949-1952, 1982.

Kawada, S.: Induced velocity by helical vortices, Journal of Aeronautical Sciences, 36, 86-87, 1936.

Krogstad, P. Å., Adaramola, M. S.: Performance and near wake measurements of a model horizontal axis wind turbine. Wind Energy, 15(5), 743-756, 2012.

van Kuik, G. A. M.: The fluid dynamic basis for actuator disc and rotor theories. IOS Press, 2018.

van Kuik, G. A. M.: On the velocity at wind turbine and propeller actuator discs, Wind Energy Science, 5(3), 855-865, 2020.

Limacher, E.J., Wood, D.H.: An impulse-based derivation of the Kutta-Joukowsky equation for wind turbine thrust, Wind Energy Science, 6(1), 191-201, 2020.

McCutchen, C. W.: A theorem on swirl loss in propeller wakes. Journal of Aircraft, 22(4), 344-346, 1985.

Noca, F.: On the time-dependent fluid-dynamic forces on bluff bodies. PhD thesis, California Institute of Technology, 1997.

Okulov, V. L., Sørensen, J. N. : Refined Betz limit for rotors with a finite number of blades. Wind Energy, 11, 415-426, 2008.

Ricca, R. L.: The effect of torsion on the motion of a helical vortex filament. Journal of Fluid Mechanics, 273, 241-259, 1994.

Saffman, P.G.: Vortex Dynamics, C.U.P., 1992.

Segalini, A., Alfredsson, P. H. : A simplified vortex model of propeller and wind-turbine wakes. Journal of Fluid Mechanics, 725, 91, 2013.

Sørensen, J. N.: General Momentum Theory for Horizontal Axis Wind Turbines, Springer International Publishing, Heidelberg, doi:10.1007/978-3-319-22114-4, 2016.

Wood, D. H.: Including swirl in the actuator disk analysis of wind turbines. Wind Engineering, 31(5), 317-323, 2007.

Wood, D. H.: Maximum wind turbine performance at low tip speed ratio. Journal of Renewable and Sustainable Energy, 7(5), 053126, 2015.

Wood, D. H., Okulov, V. L. : Nonlinear blade element-momentum analysis of Betz-Goldstein rotors. Renewable Energy, 107, 542-549, 2017.

Wood, D. H., Okulov, V. L., Vaz, J. R. P.: Calculation of the induced velocities in lifting line analyses of propellers and turbines. Ocean Engineering, 235, 109337, 2021.